

A dual-scale sub-grid closure for LES of phase interfaces with phase change

By A. Goodrich[†], D. Kedelty[†] AND M. Herrmann[†]

Advances to a dual-scale modeling approach are presented for a turbulent phase interface with phase change in a large eddy simulation (LES) framework. Applying a spatial filter operator to the governing equations introduces several unclosed sub-filter terms that require modeling. In the dual-scale approach, interface-related sub-filter terms are not closed by a proposed model but instead are closed exactly with an explicit filter of a fully resolved realization of the interface. The fully resolved interface realization is retained with a high-resolution overset mesh via the refined local surface grid method (Herrmann 2008), and interface transport is carried out with an unsplit geometric volume-of-fluid method (Owkes & Desjardins 2014). Transport of the fully resolved interface requires a fully resolved velocity field and thus requires modeling from the LES filtered velocity. The fully resolved velocity is the sum of the filtered LES velocities and modeled sub-filter velocity components due to phase change, turbulent eddies and surface tension. Phase change velocities are evaluated locally with a prescribed evaporation speed and an interface normal vector from the fully resolved interface realization. Sub-filter turbulent fluctuation velocities are generated from a spectrally enriched differential filter (Bassenne *et al.* 2019) and sub-filter surface tension forces are modeled with a phenomenological spring and damper model (Herrmann 2013). Detailed numerical simulations of an evaporating, initially planar interface, subjected to homogeneous isotropic turbulence, are presented and the interplay between phase change and surface tension is studied. Dual-scale results are presented and compared against the DNS.

1. Introduction

Phase interface dynamics in turbulent flows play a critical role in many engineering and industrial applications. Industrial paint application, pesticide dispersal and internal combustion engines all heavily rely on rapid liquid atomization for efficiency and performance optimization. Combustion, for example, requires a specific gaseous fuel-air mixture to optimize engine performance, pollutant production and efficiency. Details of the primary atomization, phase change and mixing processes of turbulent phase interfaces are therefore of great importance in achieving cleaner, more sustainable energy conversion.

Predicting liquid fuel atomization and evaporation in turbulent flows remains a particularly challenging task with presently available numerical methods and models. Detailed numerical simulations (DNS) can shed light on the underlying physical phenomena that govern the atomization and evaporation of turbulent phase interfaces. However, due to the enormous range of spatial and temporal scales that must be resolved to capture all the relevant dynamics, DNS require a staggering amount of computational resources that are unavailable to many design engineers. Even with a large amount of computational resources at hand, DNS have so far been limited to flows with moderate Reynolds and

[†] School for Engineering of Matter, Transport and Energy, Arizona State University

Weber numbers and engineering designs with simple geometries. A need therefore exists for a toolset that is capable of accurate atomization predictions and well-suited for engineering studies. For this purpose, modeling approaches compatible within the large eddy simulations (LES) framework are needed for studying primary atomization.

Several LES models for turbulent immiscible interfaces have been proposed in the past (Labourasse *et al.* 2007; Toutant *et al.* 2008, 2009a,b). Prior LES models relied on the existence of a universality of scales to infer small sub-grid-scale motion from the resolved large-scale features of the flow. While this modeling technique has proven successful in single-phase turbulent flows due to the existence of the energy cascade, it remains an open question whether a similar universality can be exploited in a traditional LES closure model for phase interfaces.

Viscosity is known to consistently dissipate fluid motion on small scales in turbulent flows, and like viscosity, surface tension forces tend to increase at small scales given the larger interfacial curvature. However, surface tension can either shrink or amplify surface corrugations via instability mechanisms like Kelvin-Helmholtz (Kelvin 1871; Helmholtz 1868) or Rayleigh-Plateau (Rayleigh 1878; Plateau 1873). At present time it is unclear whether the resolved filtered interface geometry can be used to reliably predict the dual nature of surface tension on the sub-filter scales.

Regarding phase change in DNS of primary atomization, the current state of the art is to neglect phase change everywhere except atomized drops. Phase change is only accounted for in spray regions that are usually modeled with Lagrangian point-particle methods. This is typically deemed acceptable since liquid evaporation will be predominantly governed by the large amount of interfacial area in the spray region. However, a non-trivial amount of fuel vapor emerging from the near-nozzle region could contribute to flame stabilization and play an important role in combustion applications. Details of the evaporated fuel vapor strongly depend on the available surface area for phase transition, and therefore, LES approaches require models of the sub-filter interfacial area that account for sub-filter turbulent fluctuations, shear and accelerational instabilities, and surface tension forces.

Since details of the sub-filter interface geometry in the traditional LES approach are unavailable, the dual-scale approach was proposed to provide a fully resolved realization of the sub-filter interface geometry (Herrmann 2008) and properly handle the sub-filter effects. In this work, a phase change model compatible with the dual-scale approach is tested in a turbulent environment with a variety of evaporation and surface tension conditions.

2. Governing equations

The governing equations for an unsteady, incompressible, immiscible, two-fluid system with a unit density ratio and unit viscosity ratio are the non-dimensional Navier-Stokes equations given by

$$\frac{\partial \mathbf{u}}{\partial t} + \nabla \cdot (\mathbf{u} \otimes \mathbf{u}) = -\nabla p + \frac{1}{Re} \nabla \cdot [(\nabla \mathbf{u} + \nabla^T \mathbf{u})] + \frac{1}{We} \kappa \delta(\mathbf{x} - \mathbf{x}_f) \mathbf{n}, \quad (2.1)$$

where \mathbf{u} is the velocity, Re is the Reynolds number, We is the Weber number, p is the pressure, κ is the interfacial curvature, δ is the Dirac delta function and \mathbf{n} is a unit vector normal to the interface. Additionally, the continuity equation constrains the velocity field to be divergence-free,

$$\nabla \cdot \mathbf{u} = 0. \quad (2.2)$$

The volume-of-fluid (VoF) scalar, defined as $\psi = 0$ in the gas phase and $\psi = 1$ in the liquid phase, is used to distinguish phases. Transport of ψ is governed by

$$\frac{\partial \psi}{\partial t} = -(\mathbf{u} + s_L \mathbf{n}) \cdot \nabla \psi = -\nabla \cdot ((\mathbf{u} + s_L \mathbf{n}) \psi) + \psi \nabla \cdot (\mathbf{u} + s_L \mathbf{n}). \quad (2.3)$$

2.1. Filtered governing equations

Employing a spatial filter to Eqs. (2.1)-(2.2) and assuming the filter commutes with space and time derivatives yield the filtered governing equations,

$$\frac{\partial \bar{\mathbf{u}}}{\partial t} + \nabla \cdot (\bar{\mathbf{u}} \otimes \bar{\mathbf{u}}) = -\nabla \bar{p} + \frac{1}{Re} \nabla \cdot [(\nabla \bar{\mathbf{u}} + \nabla^T \bar{\mathbf{u}})] + \bar{\mathbf{T}}_\sigma + \nabla \cdot \boldsymbol{\tau}, \quad (2.4)$$

$$\nabla \cdot \bar{\mathbf{u}} = 0, \quad (2.5)$$

where $\overline{(*)}$ denotes the spatial filtering operator, and

$$\bar{\mathbf{T}}_\sigma = \frac{1}{We} \overline{\kappa \delta(\mathbf{x} - \mathbf{x}_f) \mathbf{n}}, \quad (2.6)$$

$$\boldsymbol{\tau} = \bar{\mathbf{u}} \otimes \bar{\mathbf{u}} - \overline{\mathbf{u} \otimes \mathbf{u}}, \quad (2.7)$$

where $\bar{\mathbf{T}}_\sigma$ is due to surface tension and $\boldsymbol{\tau}$ is due to sub-filter-scale momentum transport. Typically, the filtered VoF scalar is obtained by taking an explicit filter of Eq. (2.3), which results in additional sub-filter terms. However, in the dual-scale approach Eq. (2.3) is solved directly and the filtered volume fraction $\bar{\psi}$ can be calculated by explicitly filtering

$$\bar{\psi} = \int \mathcal{G}(\mathbf{x}) \psi d\mathbf{x}, \quad (2.8)$$

where \mathcal{G} is a normalized spatial filter function integrated over the filter volume.

3. The dual-scale approach to modeling sub-filter interface dynamics

Instead of relying on a cascade mechanism to model the unclosed sub-filter interface-related terms \mathbf{T}_σ and $\boldsymbol{\tau}$, a fully resolved realization of the phase interface is maintained on a high-resolution overset mesh (Herrmann & Gorokhovski 2008). The fully resolved realization of the interface is expressed in terms of the VoF scalar ψ , and the filtered interface is attained by taking an explicit filter of ψ [Eq. (2.8)]. Although this procedure describes an exact closure of the sub-filter terms, it shifts the modeling task to maintaining a fully resolved realization of the interface geometry. To advance the fully resolved realization, the fully resolved velocity $\mathbf{u} = \bar{\mathbf{u}} + \mathbf{u}_{sgs}$ is substituted into the fully resolved ψ transport equation [Eq. (2.3)],

$$\frac{\partial \psi}{\partial t} = -\nabla \cdot ((\bar{\mathbf{u}} + \mathbf{u}_{sgs}) \psi) + \psi \nabla \cdot (\bar{\mathbf{u}} + \mathbf{u}_{sgs}). \quad (3.1)$$

Thus the only term that requires modeling is \mathbf{u}_{sgs} , which has been proposed to be linearly decomposed into

$$\mathbf{u}_{sgs} = \mathbf{u}' + \mathbf{u}_\sigma + \delta\mathbf{u} + \mathbf{u}_a + s_L\mathbf{n}, \quad (3.2)$$

where \mathbf{u}' is due to sub-filter turbulent fluctuations, \mathbf{u}_σ is due to sub-filter surface tension forces, $\delta\mathbf{u}$ is due to the relative shear between phases, \mathbf{u}_a is due to accelerational instabilities, and $s_L\mathbf{n}$ is the sub-filter interface normal velocity due to mass transfer through the interface caused by phase change.

3.1. The sub-filter velocities

The sub-filter turbulent fluctuation velocities \mathbf{u}' are reconstructed from the LES filter scale velocities $\bar{\mathbf{u}}$ using a spectrally enriched differential filter (SDF) proposed by Bassenne *et al.* (2019). Sub-filter surface tension velocities \mathbf{u}_σ are reconstructed using a phenomenological model that invokes a spring and damper analogy to reconstruct the effects of surface tension (Herrmann 2013). Velocities resulting from the reconstruction models are not divergence free and therefore require a projection/correction step in a narrow band surrounding the fully resolved interface. Sub-filter shear and accelerational instabilities, although not used in the present numerical experiments, are modeled using a vortex sheet method (Herrmann 2005) extended to geometric VoF interface advection schemes.

The velocities due to mass transfer through the interface $s_L\mathbf{n}$ are modeled following a premixed flame analogy (Williams 1985), where s_L is an evaporation speed (analogous to a laminar burning speed) and \mathbf{n} is the fully resolved interface normal vector. For the initial evaluation of the phase change model presented here, s_L will be prescribed uniformly as $s_L = s_L^0$ for each simulation; however, in principle the evaporation speed can be modeled with filter-scale quantities like temperature and species mass fractions.

4. Numerical methods

The filtered Navier-Stokes equations presented in Eqs. (2.4)-(2.5) are solved using NGA, a structured, staggered, finite difference flow solver that employs the fractional step method (Desjardins *et al.* 2008). Tracking the fully resolved phase interface realization is accomplished by solving Eq. (2.3) on a high-resolution auxiliary Cartesian grid maintained with the refined local surface grid (RLSG) framework (Herrmann 2008).

The VoF scalar in Eq. (3.1) is advanced in time using the unsplit geometric transport scheme of Owkes & Desjardins (2014). The method ensures that the VoF scalar remains bounded and discretely conserves volume for each phase in the absence of phase change. Within each computational cell the interface is represented with piecewise linear interface construction (PLIC) using analytical formulas (Scardovelli & Zaleski 2000) and efficient least-squares VoF interface reconstruction algorithm (ELVIRA)-estimated normals (Pilliod & Puckett 2004).

In the dual-scale approach, the highly resolved narrow-band Cartesian overset mesh uses the RLSG framework with a grid spacing h_G that is independent of the underlying LES flow solver grid with mesh spacing h . The refinement level of the RLSG is calculated from $r = \log_2(h/h_G)$, and the RLSG spacing h_G must be sufficiently small to maintain a fully resolved realization of the phase interface.

In the SDF model (Bassenne *et al.* 2019), sub-filter turbulent velocities are calculated via a recursive refinement and spectral enrichment procedure repeated r times to the RLSG mesh. Trilinear interpolation is used to refine between successive grid levels 2Δ and Δ , and since the LES flow solver uses a staggered mesh, face-centered velocities are

refined onto cell vertices. During intermediate refinement steps this is advantageous for velocity gradient calculations needed in the spectral enrichment step. However, in the final refinement step, velocities are interpolated from cell vertices to cell faces where they are needed for the staggered RLSG mesh.

Sub-filter surface tension velocities \mathbf{u}_σ are evaluated using the geometry of the fully resolved realization of the phase interface. The phenomenological model captures surface tension forces as a spring and damper system. Originally proposed by Herrmann (2013), the model has since been improved upon with modifications that extend its capability to scenarios where the filtered interface has no mean curvature but the sub-filter interface has sub-filter corrugations. Numerically, \mathbf{u}_σ is collocated at cell centers with the interface curvature κ and interface normal vector \mathbf{n} , but since κ and \mathbf{n} are only available at cells that contain an interface, a problem arises when trying to calculate \mathbf{u}_σ away from the interface. Thus, a fast sweeping method (Zhao 2005) is employed to extend the surface tension velocities away from the interface. Finally, the cell-centered surface tension velocities are computed at cell faces with an arithmetic average.

Neither the SDF model for turbulent fluctuation velocities nor the surface tension velocities are constrained to be divergence free, but the unsplit geometric transport scheme of Owkes & Desjardins (2014) requires a divergence-free velocity field to ensure both conservation and boundedness of the VoF scalar. To ensure $\nabla \cdot (\mathbf{u}' + \mathbf{u}_\sigma) = 0$, $(\mathbf{u}' + \mathbf{u}_\sigma)$ is projected into the subspace of divergence-free velocity fields using a standard projection/correction step common to the fractional step method. Note that the resulting Poisson system that projects $\mathbf{u}' + \mathbf{u}_\sigma$ is constructed on a band of RLSG contained in LES cells surrounding the interface. RLSG cell faces that do not neighbor other cells within the active band have a uniform correction velocity added to ensure $\overline{(\mathbf{u}' + \mathbf{u}_\sigma)} = \bar{\mathbf{u}}$. The required Poisson system is solved using the Aztec package found in the Trilinos software library (The Trilinos Project Team 2020).

The velocities due to phase change $s_L \mathbf{n}$ simply require the interface normal vector to be computed from the fully resolved interface realization. Using the ELVIRA-estimated normals from the unsplit geometric transport scheme appears to be the obvious choice since they are readily available and provide consistency with VoF transport. However, the phase change velocities will be non-solenoidal along curved interfaces because $\nabla \cdot (s_L \mathbf{n}) = s_L \nabla \cdot \mathbf{n} = s_L \kappa$. Moreover, ELVIRA-estimated normals can change substantially from cell to cell in under-resolved and highly curved interface segments. Furthermore, the VoF transport scheme employs a correction factor for non-solenoidal velocity fields that takes the form

$$\psi^{n+1} = \frac{\psi^n + \Delta\psi}{1 - \Delta t \nabla \cdot \mathbf{u}}, \quad (4.1)$$

where $\Delta\psi$ is the net geometrically captured flux of liquid volume into/out of the cell computed from Owkes & Desjardins (2014). Since $\mathbf{u}' + \mathbf{u}_\sigma$ are projected into the solenoidal subspace with a projection/correction step, the denominator simplifies to $1 - \Delta t s_L \nabla \cdot \mathbf{n}$, and gradients of ELVIRA normals were found to generate large non-physical corrections, especially in under-resolved and highly curved interface segments. Not only do small atomized drops produce high-curvature regions, but Huygen's principle states that convex interface segments will lead to sharp cusps on an interface propagating normal to itself. Therefore, highly curved regions of the interface are inevitable and the sharp jumps in ELVIRA normals will generate unacceptably high error in the VoF correction term.

To avoid these issues with ELVIRA, the normal vector is calculated using a recon-

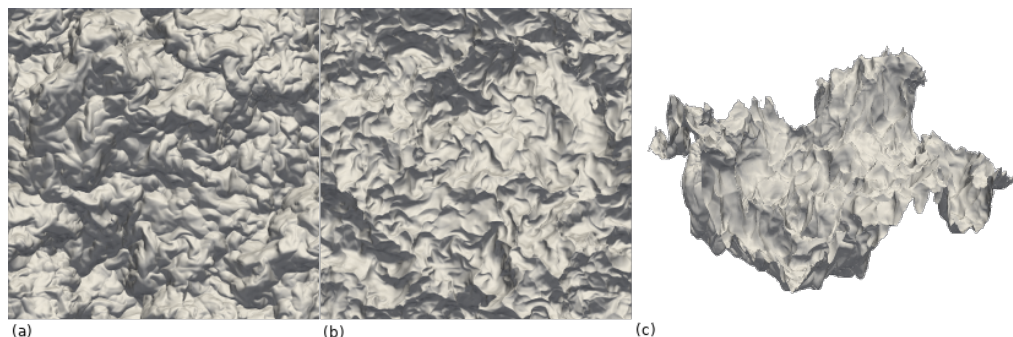


FIGURE 1. An initially flat interface subjected to HIT with $Re_\lambda = 162$, $We = \infty$ and a uniform evaporation speed $s_L^0/u' = 0.85$ at $t/t_L = 1$ as viewed from (a) the liquid side (b) the gas side. Panel (c) presents an isometric view.

structed level set function. At each timestep the level set is initialized in interface cells with the distance between the PLIC and the cell center, and subsequently extended to a band surrounding the interface with a fast sweeping method (Zhao 2005). The interface normal vector \mathbf{n} is computed from the level set with second-order central differences and arithmetically averaged to cell faces. Normals computed with the reconstructed level set provide substantially smoother gradients for the VoF correction factor than ELVIRA-estimated normals do.

5. Results and discussion

As a preliminary test of the phase change velocity model, the classical D^2 -law proposed by Langmuir (1918) to compute drop evaporation rates will be used as inspiration. For this test case, a unit density drop of initial radius $r_0 = 1/4$ is placed in a unit square domain with an evaporation speed $s_L = \kappa$. Under these conditions the mass of the drop m is governed by

$$\frac{m}{m_0} = 1 - \frac{2t}{r_0^2}, \quad (5.1)$$

where m_0 is the initial mass of the drop and t is time. In the numerical experiment, a 128^2 grid is employed and the mass of the drop is tracked at every timestep by integrating $m(t) = \rho \int_V \psi(t) dV$ over the entire domain. Under the prescribed conditions, the coefficient in front of t should theoretically be $2/r_0^2 = 32$ and the drop would fully evaporate at $t_f = 0.03125$. From the numerical experiment, a value of $2/r_0^2 \approx 31.982$ is found by fitting a line to the time series data with the method of least squares from $t = 0$ to $t = t_f$. This differs from the theoretical value by only 0.06% and thus the proposed phase change velocity model shows excellent agreement.

5.1. Phase change of an interface subjected to homogeneous isotropic turbulence

To obtain verification data for evaluating the LES sub-grid closure model and to study the physical phenomena introduced with the inclusion of phase change, DNS of decaying homogeneous isotropic turbulence (HIT) with constant phase change speed are performed. In the following test cases, an initially flat interface is placed in the center of a triply periodic box of decaying HIT. The prescribed evaporation speed varies between $s_L^0/u' = 0.17$, 0.34, 0.85 and 1.7, and for each evaporation speed the surface tension

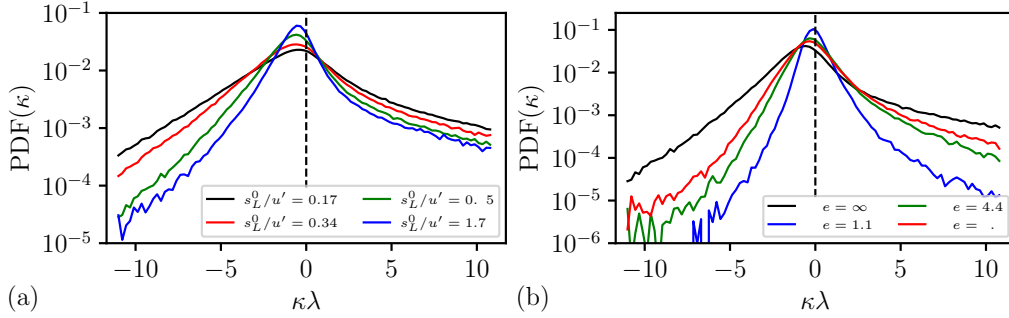


FIGURE 2. Probability density of interfacial curvature κ at $t/t_L = 1$ of an initially flat interface subjected to HIT with $Re_\lambda = 162$ with (a) various evaporation speeds s_L^0/u' and $We = \infty$ and (b) various We number conditions and $s_L^0/u' = 0.85$.

varies between $We = 1.1, 4.4, 8.8$ and ∞ . For the sake of brevity, results from only a few cases are presented. A fully developed isotropic turbulence field of $Re_\lambda = 162$ (Chiodi & Desjardins 2017) is used as initial conditions for the velocity field. Density and viscosity ratios are set to unity and a 512^3 grid is employed for all DNS results. Since evaporation speeds are prescribed uniformly for each test case and fluid property ratios are set to unity, expansion effects are absent.

Note that applying an evaporation speed normal to an interface will move the filtered interface position in the simulation domain. Due to the triply periodic nature of the domain, this should theoretically be no issue for a passive interface; however, the interface initialization is employed with a Heaviside step function of the VoF scalar. Therefore, the periodic condition is broken in the interface normal direction for the VoF scalar. In past studies employing dual-scale in triply periodic HIT, the VoF scalar is only advected in a narrow-band surrounding the interface and the interface does not reach the upper/lower boundaries of the domain within the simulated time. This problem cannot be so easily avoided in the simulations here, since the evaporation speeds employed will transport the interface to domain boundaries well before a single eddy turnover time. To resolve these concerns and anchor the filtered interface position in the center of the domain, a linear transformation velocity u_T is uniformly applied to the VoF advection velocities at each timestep. The linear transformation velocity is numerically evaluated at each timestep n by

$$u_T^n = u_T^{n-1} - \frac{\langle \psi \rangle_{1/2}^n - \langle \psi \rangle_{1/2}^{n-1}}{\Delta t}, \quad (5.2)$$

where $\langle \psi \rangle_{1/2}$ is the $\psi = 1/2$ iso-surface linearly interpolated from the homogeneously filtered VoF field.

Figure 1 shows an example of the interface after a full eddy turnover time from various viewpoints. When viewed from the liquid side, the interface shows more smooth and rounded features as opposed to the sharp cusps visible from the gas side. This asymmetry is easily explained by Huygen's principle, which states that concave regions (seen from the liquid side) of an interface will flatten out and convex regions (seen from the gas side) will shrink and form sharp cusps under self-normal propagation.

Figure 2(a) shows the area-weighted probability density of the interface curvature κ after one eddy turnover time. Increasing the evaporation speed clearly has the effect of asymmetrically skewing the probability density function (PDF) of curvature to negative

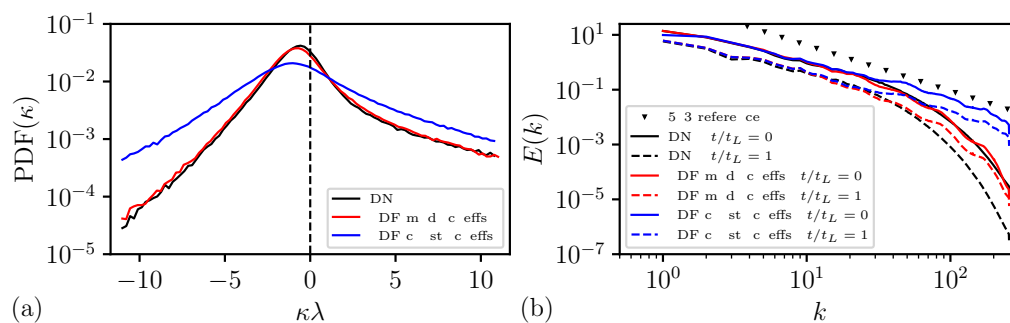


FIGURE 3. Results from an LES of an initially flat interface subjected to HIT with $Re_\lambda = 162$, $We = \infty$ and a uniform evaporation speed $s_L^0/u' = 0.85$. (a) Probability density of curvature κ at $t/t_L = 1$ and (b) the kinetic energy spectrum of velocity fields from DNS and the SDF model.

values; moreover the tails of the PDF become increasingly asymmetric with increasing evaporation speeds. These observations are consistent with Figure 1 and Huygen's principle since the concave regions (negative curvature) flatten out and the convex regions (positive curvature) form sharp cusps. Small-scale corrugations are rapidly smoothed out with increasing evaporation speed, resulting in a significantly lower probability of high-curvature regions for both negative and positive curvature values. However, due to cusp formation the probability reduction is more pronounced in negative curvature values.

Figure 2(b) shows results where the evaporation speed is held constant at $s_L^0/u' = 0.85$ and surface tension is successively increased between cases. Increasing surface tension restores the PDF of curvature back to a more symmetric curve. Since surface tension smooths out high-wavenumber corrugations, the probability of high curvature values is greatly decreased. This can be easily seen in the tails of the PDF of curvature in Figure 2(b). Although increasing surface tension greatly diminishes the presence of sharp cusps, their fingerprint is still present in the PDF since the high positive curvature values are statistically more prevalent than high negative values.

An LES of the same flow conditions as the DNS was conducted with the dual-scale approach using a 512^3 grid for the refined overset mesh and a 32^3 grid for the LES flow solver grid. Figure 3(a) shows the PDF of curvature for both the LES and DNS cases, and clearly in the SDF constant coefficients case there is a notable discrepancy between the results. In the aforementioned case, the SDF model for turbulent fluctuation velocities uses constant parameters that generate the $-5/3$ power law throughout the kinetic energy spectrum. As shown in Figure 3(b), using these constant coefficients generates velocities that follow the $-5/3$ power law throughout the entire kinetic energy spectrum at both the initial and final steps of the computation. This has the adverse effect of generating velocities with too high kinetic energy at small scales and ignores the viscous sub-range present in the DNS. Due to the increased kinetic energy at small scales, using the SDF with constant coefficients shows a statistically higher prevalence of high curvature values in Figure 3(a).

The parameters used in the SDF model can be tuned to account for the viscous sub-range present in the DNS. Thus, in Figure 3(b) the SDF-modified coefficients case initially shows excellent agreement in the kinetic energy spectrum and throughout the viscous sub-range. At the final time, however, the DNS kinetic energy spectrum has changed since the HIT is not forced at the large scales and naturally decays over time. Since the SDF parameters are tuned to the initial kinetic energy spectrum, the accuracy of

the SDF-modified coefficients case slightly degrades over time and begins overpredicting kinetic energy in the viscous sub-range. However, the kinetic energy accuracy is still a marked improvement over using constant coefficients as shown in Figure 3(b).

In the absence of the viscous sub-range, the competition between high-wavenumber eddies and evaporation velocities is tipped in favor of the high-wavenumber eddies, and thus the high-curvature corrugations are statistically more active in the SDF constant coefficients case. Inclusion of the viscous sub-range is therefore critically important for accurately predicting the interface statistics as shown in Figure 3(a). Using the SDF model with modified coefficients rather than constant coefficients is a substantial improvement and shows excellent agreement with the DNS.

A finite-Weber-number LES is notably absent from present results. In the process of testing the dual-scale approach with surface tension, it was found that previous implementations of the projection/correction step can unintentionally lead to adverse grid imprints on the interface. Therefore, finite-Weber-number LES have not been included, and future work includes development of an improved projection/correction implementation that circumvents grid imprints.

6. Conclusions

A dual-scale approach for modeling turbulent phase interface dynamics with phase change that is capable of accurately reproducing geometric interface statistics is presented. Instead of proposing closure models for the various sub-filter effects due to phase interfaces, an exact closure is presented wherein a fully resolved interface realization is explicitly filtered. A high-resolution overset mesh is employed to capture the fully resolved interface realization and to provide explicitly filtered interface quantities where necessary. DNS of an initially planar interface subjected to HIT provide insight into the behavior of turbulent phase interfaces and the interplay between phase change and surface tension. Results show that the presence of phase change velocities asymmetrically favors large concave regions of low curvature and small convex regions of high curvature. Furthermore, the presence of surface tension has a restoring effect on this asymmetry and increasing surface tension produces increasingly symmetric curvature statistics. Comparisons between dual-scale and DNS show that capturing the viscous sub-range of the kinetic energy spectrum is critically important for producing accurate interface statistics. Dual-scale results compare favorably with DNS in the infinite-Weber-regime and an improved projection/correction step for sub-filter surface tension velocities has been identified as future work.

Acknowledgments

The authors acknowledge use of computational resources from the Yellowstone cluster awarded by the National Science Foundation to CTR.

REFERENCES

- BASSENNE, M., ESMAILY, M., LIVESCU, D., MOIN, P. & URZAY, J. 2019 A dynamic spectrally enriched subgrid-scale model for preferential concentration in particle-laden turbulence. *Int. J. Multiph. Flow* **116**, 270–280.
- CHIODI, R. & DESJARDINS, O. 2017 DNS database of turbulent phase interfaces. *Private Communication*.

- DESJARDINS, O., BLANQUART, G., BALARAC, G. & PITSCH, H. 2008 High order conservative finite difference scheme for variable density low Mach number turbulent flows. *J. Comput. Phys.* **227**, 7125–7159.
- HELMHOLTZ, H. 1868 On discontinuous movements of fluids. *Philos. Mag.* **36**, 337–346.
- HERRMANN, M. 2005 A Eularian level set/vortex sheet method for two-phase interface dynamics. *J. Comput. Phys.* **203**, 539–571.
- HERRMANN, M. 2008 A balanced force refined level set grid method for two-phase flows on unstructured flow solver grids. *J. Comput. Phys.* **227**, 2674–2706.
- HERRMANN, M. 2013 A sub-grid surface dynamics model for sub-filter surface tension induced interface dynamics. *Comput. Fluids.* **87**, 92–101.
- HERRMANN, M. & GOROKHOVSKI, M. 2008 An outline of an LES subgrid model for liquid/gas phase interface dynamics. *Proceedings of the Summer Program*, Center for Turbulence Research, Stanford University, pp. 171–181.
- KELVIN, L. 1871 Hydrokinetic solutions and observations. *Philos. Mag.* **42**, 362–377.
- LABOURASSE, E., LACANETTE, D., TOUTANT, A., LUBIN, P., VINCENT, S., LEBAGUE, O., CALTAGIRONE, J. & SAGUAT, P. 2007 Towards large eddy simulations of isothermal two-phase flows: governing equations and *a priori* tests. *Int. J. Multiph. Flow* **33**, 1–39.
- LANGMUIR, I. 1918 The evaporation of small spheres. *Phys. Rev.* **12**, 368.
- OWKES, M. & DESJARDINS, O. 2014 A computational framework for conservative, three-dimensional, unsplit, geometric transport with application to the volume-of-fluid (VOF) method. *J. Comput. Phys.* **270**, 587–612.
- PILLIOD, J. E. & PUCKETT, E. G. 2004 Second-order accurate volume-of-fluid algorithms for tracking material interfaces. *J. Comput. Phys.* **199**, 456–502.
- PLATEAU, J. 1873 Experimental and theoretical statics of liquids subject to molecular forces only. *Gauthier-Villars* **2**, 248–307.
- RAYLEIGH, L. 1878 On the instability of jets. *P. Lond. Math. Soc.* **s1-10**, 4–13.
- SCARDOVELLI, R. & ZALESKI, S. 2000 Analytical relations connecting linear interfaces and volume fractions in rectangular grids. *J. Comput. Phys.* **164**, 228–237.
- THE TRILINOS PROJECT TEAM. 2020 The trilinos project website. <https://trilinos.github.io>
- TOUTANT, A., CHANDESRI, M., JAMET, D. & LEBAGUE, O. 2009a Jump conditions for filtered quantities at an under-resolved discontinuous interface. Part 1: theoretical development. *Int. J. Multiph. Flow* **35**, 1100–1118.
- TOUTANT, A., CHANDESRI, M., JAMET, D. & LEBAGUE, O. 2009b Jump conditions for filtered quantities at an under-resolved discontinuous interface. Part 2: *a priori* tests. *Int. J. Multiph. Flow* **35**, 1119–1129.
- TOUTANT, A., LABOURASSE, E., LEBAGUE, O. & SIMONIN, O. 2008 DNS of the interaction between a deformable buoyant bubble and a spatially decaying turbulence: *a priori* tests for LES two-phase flow modelling. *Comput. Fluids* **37** 877–886.
- WILLIAMS, F. A. 1985 *Combustion Theory*. Westview Press.
- ZHAO, H. 2005 A fast sweeping method for Eikonal equations. *Math. Comput.* **74**, 603–627.